CHAPTER 4: INFLUENCES ON THE CARBONATE HYDROCHEMISTRY OF MOUND SPRING ENVIRONMENTS, LAKE EYRE SOUTH REGION, SOUTH AUSTRALIA

This chapter has previously been published as the following paper:

Keppel, M.N., Post, V.E.A., Love, A.J., Clarke, J.D.A., Werner, A.D., 2012b. Influences on the carbonate hydrochemistry of mound spring environments, Lake Eyre South region, South Australia. Chemical Geology, 296-297: 50-65.

Abstract

Mound spring structures composed of tufa precipitated from near-ambient temperature springwaters are rare; consequently, the hydrochemical evolution of the water and the processes that control carbonate deposition in these systems are not well understood. This study analysed the water from three mound springs in an arid environment in the vicinity of Lake Eyre South, South Australia. Samples were tested for major ion chemistry and stable isotope ratios of water ($^{2}H/^{1}H$ and $^{18}O/^{16}O$). Most CO_2 degasses from water (i) before emergence as it ascends in the fracture-derived spring conduit system below the spring opening and (ii) after emergence in the turbulent upper tail environment between the spring vent pool and the tail delta. However, modern carbonate precipitation was generally restricted to tail delta environments, spatially disconnected from the areas of strongest CO_2 degassing. In addition to CO_2 degassing and carbonate precipitation, evapotranspiration and heterotrophy were inferred to be processes controlling the chemical evolution of water flowing through the tail delta. Based on considerations of the geometry of the tail delta and evapotranspiration rates, it was inferred that infiltration is an important

process in determining the tail delta size and hence the morphology of the mound spring environment. A reactive transport model was used to assess the importance of these processes for the evolution of carbonate hydrochemistry. The model outcomes showed that water loss via evapotranspiration does not significantly affect tufa precipitation, despite the springs being located within an arid environment. Heterotrophy was considered in the model in order to reproduce observed pH and carbonate concentrations, highlighting the role of vegetation in controlling the water chemistry. The modelling approach adopted here provides a generic framework for the analysis of calcareous spring deposits and places quantitative constraints on data-based process conceptualisation.

4.1 Introduction

Calcareous spring deposits are limestones precipitated from springwater (Jones and Renaut, 2010). As the fabric, mineralogy and geochemistry of these rocks are sensitive to the particular environmental conditions in which they form, these deposits can be important archives of information concerning palaeo-environmental conditions and have consequently been studied to understand the palaeohydrology, palaeoclimatology and neotectonics of regions where they occur (e.g. Andrews, 2006; Hancock et al., 1999; Love et al., 2009; Miner et al., 2007). However, adequate interpretation requires that the factors and processes that control the structure and morphology of these deposits are well understood.

Calcareous spring deposits in the vicinity of Lake Eyre South in South Australia are often dome-shaped and are associated with springwater discharge from the GAB. These morphological features are locally known as “mound springs” (Habermehl, 1982). The precipitation of carbonate from emergent springwater and the controls on this process are integral to the construction of these morphological features. Similar structures found elsewhere in the world are often referred to as spring mounds (e.g. Crombie et al., 1997; Linares et al., 2010). The mound springs of the GAB hold great cultural, tourist and ecological importance (e.g. Ah Chee, 2002; Leek, 2002; Ponder, 2002) and their preservation has a high priority, which requires in-depth knowledge of their formation mechanisms.

Early works concerning the carbonate hydrochemistry of calcareous spring environments by Barnes (1965), Holland et al. (1964) and Langmuir (1971) identified CO_2 degassing as the main driver for carbonate precipitation and showed that calcite super-saturation occurs due to a difference in the physio-chemical

conditions between the subsurface and the surface environment. Recently Shvartsev et al. (2007) determined that hydrolysis of aluminosilicates, producing HCO_3^- and Ca^{2+} as by-products, was also capable of forming carbonate-precipitating springwaters. However, other processes and factors have been identified that simultaneously interfere with the formation process; Herman and Lorah (1987), Lebron and Suarez (1996), Liu et al. (1995), Meyer (1984), and Pentecost (1992) found that the calcite super-saturation does not necessarily lead to immediate precipitation as there may be kinetic inhibition. Other studies have explored the particular micro-environmental conditions that may promote precipitation in nature; for instance, Chen et al. (2004), Dreybrodt and Buhmann (1991), Kano et al. (1999), Liu et al. (1995), Lorah and Herman (1988), Lu et al. (2000) and Zhang et al. (2001) all found that turbulent flow conditions will promote CO_2 degassing by reducing pressure, increasing the water surface area and reducing the diffusion boundary layer in the stream, thereby increasing the rate of $CaCO_3$ precipitation. Likewise, some studies have argued that biological processes such as photosynthesis of microbial organisms affect the precipitation of $CaCO_3$, particularly in quiescent flow conditions. Such studies include Baskar et al. (2006), González-Muñoz et al. (2010), Lee (2003) and Pentecost (1988), who inferred the importance of bio-mineralisation by isolating particular microbes in a laboratory-based setting. Gradzinski (2010), Kandianis et al. (2008), Pedley and Rogerson (2010) and Pedley et al. (2009) drew similar conclusions via a number of experiments using natural surface waters. Finally, Pedley (1994) detailed evidence from SEM, petrography and laboratory experiment to describe the role of microphyte-prokaryote biofilms in tufa accumulation. Macrophytes can impact calcareous spring deposits by providing additional substrate for the nucleation and accumulation of carbonate precipitate

(Pedley, 1992; Pentecost, 2005) and can also affect water chemistry via photosynthesis (Liu et al., 2006; Liu et al., 2008; Pentecost, 1992; Spiro and Pentecost, 1991).

Carthew et al. (2003), Carthew et al. (2006), Pedley et al. (1996), Pentecost (2005), Radke (1990) and Wright (2000) suggested that evaporation is an important factor in ambient-temperature calcareous spring deposition in semi-arid and arid environments, but hydrochemical data was not used in any of these studies to provide supporting evidence. The effect of flow conditions on carbonate precipitation has to date focused on the effects of turbulence, such as in waterfalls (e.g. Chen et al., 2004; Zhang et al., 2001) and barrages forming pool structures (e.g. Lu et al., 2000). Of most relevance to this study, Kerr and Turner (1996) grew mounds of Na_2CO_3 in a controlled laboratory environment, but the value of these experiments as a generic analogue for mound springs is limited by their design, notably the use of Na_2CO_3 rather than $CaCO_3$, and the temperature differential between "springwater" and ambient conditions, which is not necessarily encountered in field conditions.

Terminology used in the international literature to describe spring-related carbonates is diverse (Jones and Renaut, 2010); the nomenclature by Ford and Pedley (1996) has been adopted here. They defined "tufa" as a fine-grained micritic carbonate precipitated at ambient and sub-ambient water temperatures containing abundant microbial-influenced textures.

Many of the mound springs of the Lake Eyre South region are interpreted to be composed of tufa (Chapter 3; Habermehl, 1986). Despite previous references to GAB mound springs in the international literature (e.g. Ford and Pedley, 1996; Kerr and

Turner, 1996; Mudd, 2000; Pentecost, 2005; Viles and Goudie, 1990; Williams and Holmes, 1978), there is little information on the hydrochemistry of these environments. The same holds for the few detailed studies of active environments of similar features found elsewhere in the world (Linares et al., 2010; Pentecost, 2005; Pentecost and Viles, 1994).

The lack of hydrochemical data concerning the active depositional environments of mound springs renders our current understanding of the processes that control the formation of these features limited. The purpose of this study is to determine the environmental or hydrochemical conditions affecting formation and ongoing evolution of mound springs. To this aim, water samples from a number of active spring environments in the Lake Eyre South region of South Australia were collected and a novel application of reactive transport modelling was developed for the delta-shaped spring discharge fans. Additionally, evapotranspiration effects were quantified by the use of chloride (Cl^-) and stable isotope analysis. Based on the data and the model simulations, the relative contributions of CO_2 degassing and evapotranspiration to $CaCO_3$ precipitation have been quantified.

4.2 Study Area

4.2.1 Climate and hydrology

The study area is situated in an arid climate zone within the southwestern corner of the Lake Eyre Basin. The mean daily maximum temperature for the nearest town with records (Marree, Figure 4.1) is 28.4°C, whereas the mean daily minimum temperature is 13.3°C. The average annual rainfall is approximately 125 mm/year. Rainfall totals between given years can vary significantly and is predominantly in the

form of sporadic weak winter-dominated (June to August) weather events (Allan, 1990; McMahon et al., 2005). Pan evaporation rates for the Cooper Creek region of central Australia average 2.5 m/year (Hamilton et al., 2005).

Regional drainage is directed predominantly to the east towards Lake Eyre South. A small but continuous contribution to stream flow is provided by springwaters supplied by the GAB. Stream flow events derived from precipitation are infrequent (Allan, 1990).

4.2.2 Regional geology and hydrogeology

Natural groundwater spring discharge from the GAB is responsible for the formation of the spring structures that are the subject of this study. The GAB covers approximately 1.7 million km^2 of the Australian landmass (Habermehl, 1980). Recharge areas are located along the eastern seaboard and in central Australia (Figure 4.1).

For GAB groundwater recharged from the eastern seaboard, residence times between areas of recharge and discharge of between 900,000 years and 1.5 million years have been estimated using ^{36}Cl data (Torgersen, 1994), while groundwater recharged in central Australia has an estimated residence time of between 200,000 and 400,000 years inferred from ^{81}Kr data (Collon et al., 2000; Lehmann et al., 2003).

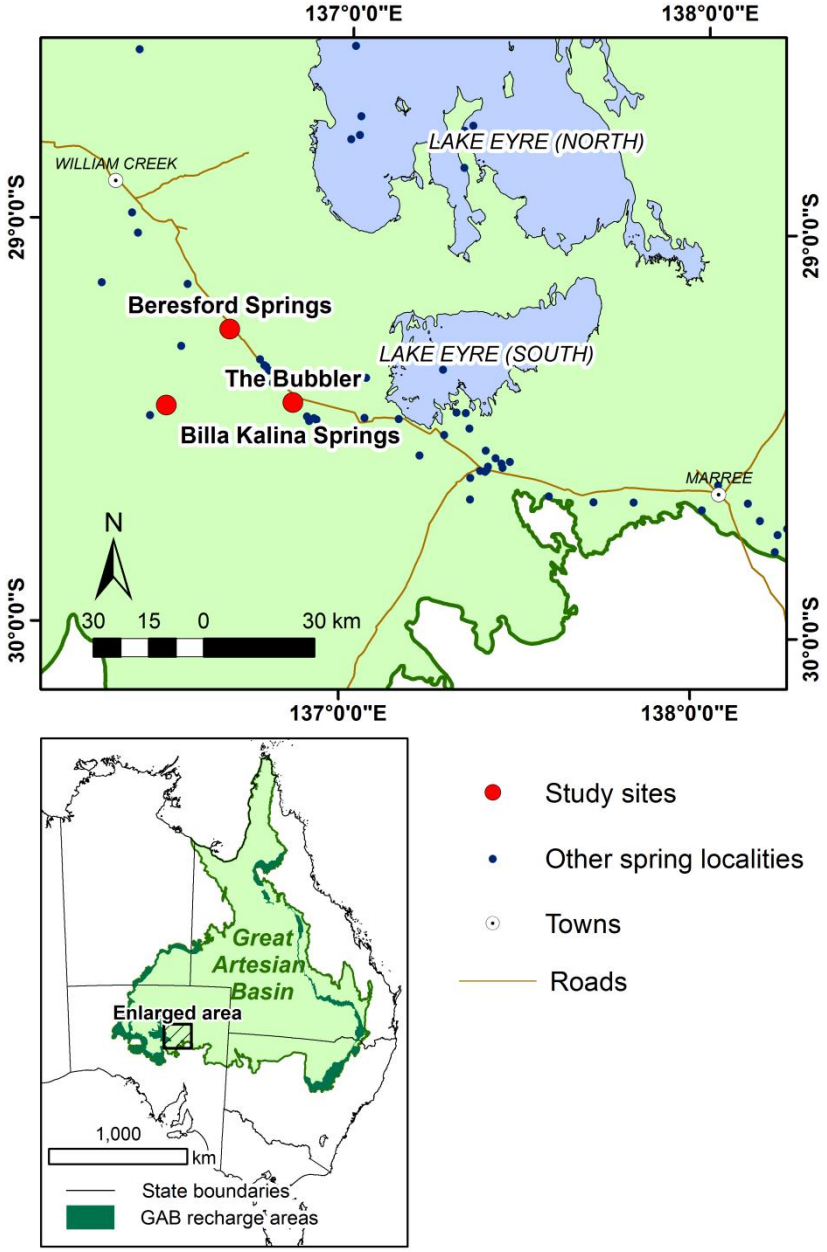

Figure 4.1: Location map of the study area, showing the locations of the sampled springs and other mound springs.

The springs located in the vicinity of Lake Eyre South are largely fed by aquifer units made up by the Cretaceous Cadna-owie Formation and the Jurassic Algebuckina Sandstone, which are generally treated as a single unit for hydrogeological purposes (Radke et al., 2000; Welsh, 2000). In the state of South Australia, the aquifer is confined by a predominantly grey marine shaly mudstone of Cretaceous age named the Bulldog Shale (Wopfner, 1972; Wopfner et al., 1970) and is commonly found sub-cropping throughout the area (Figure 4.2). The springs and the conduits connecting the aquifer with the surface are largely fault controlled (Aldam and Kuang, 1988; Krieg et al., 1991; Radke, 1990).

4.2.3 Spring sites

The springs that were investigated (Figure 4.1) were Warburton Spring, which is part of the Beresford Hill Spring complex, Billa Kalina Spring and The Bubbler, the latter being part of the Wabma Kadarbu National Park spring complex. All three studied springs possess a mound structure composed of tufa, with a central pool located over the spring vent. Billa Kalina Spring has a dome shape with relatively steep sides (Figure. 4.3A), while Warburton Spring and The Bubbler have large, low-angle shield structures (Figure 4.3B, C and D). They vary in height from 2 to 5 m from base to peak.

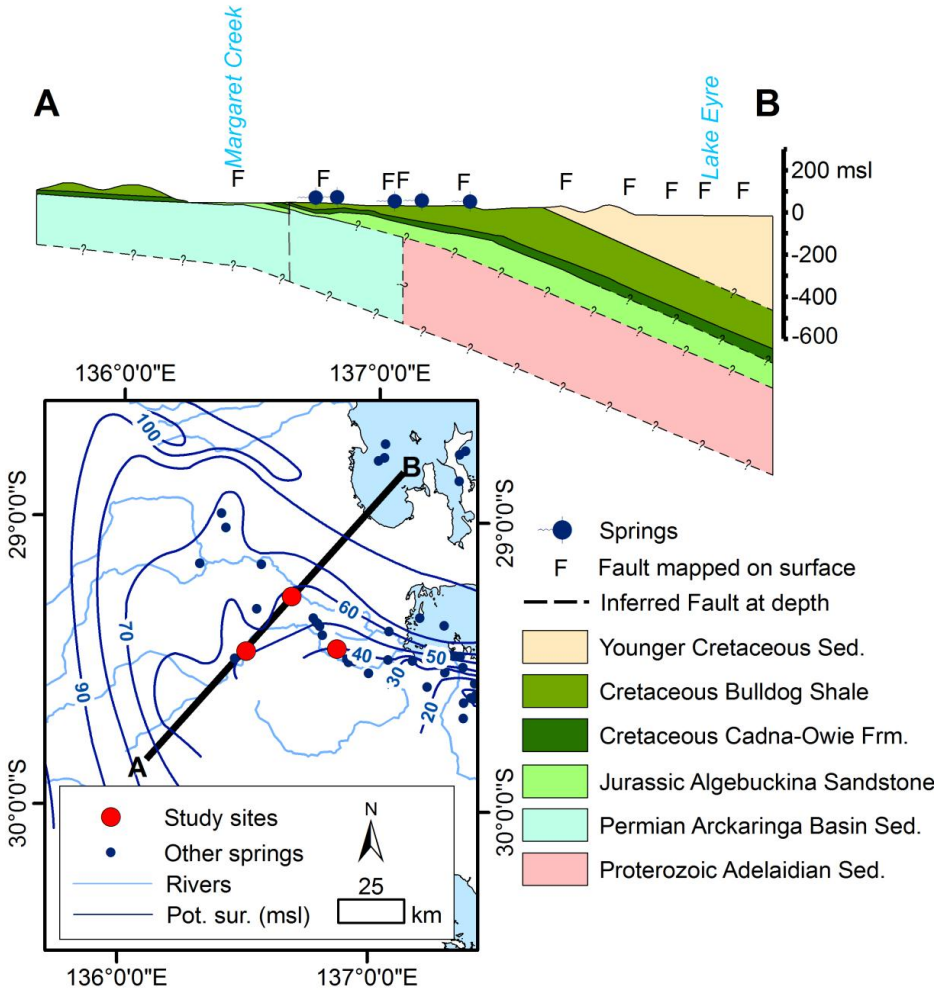

Figure 4.2: Schematic cross section through Lake Eyre South region showing various aquifer and aquitard units of the GAB and position of the springs. Section based on drilling data and mapping on published 1:250,000 map sheets (Ambrose et al., 1980; Callen et al., 1992; Williams and Krieg, 1975) as well as compiled seismic data provided by DFW. Potentiometric surface contours for GAB aquifer interpreted from data provided by DFW.

Most spring pools are well vegetated: Billa Kalina Spring is densely vegetated and has a water depth < 0.5 m, whereas the pool at Warburton Spring has a thick coverage of sedge grass that floats on >1m of water. The Bubbler is a rare exception, with its vegetation restricted to the pool perimeter; its water depth in the central part of the pool is >1 m. The mound structures at all sites are largely unvegetated and the water level in the pool is generally lower than the rim of the mound structure (Figure 4.3C).

Water from the mound pools exits via a break in the rim of the pool, otherwise known as a tail gutter or "break-out" (Fig. 3B). At some point upon exiting the mound pool, water disperses into a delta-shaped fan or "tail" (Figure 4.3D and 4.4). The pool, tail gutter and delta together form a permanent wetland environment. The largest spring environment by measure of the modern wetland included in this study is The Bubbler at 38,500 m^2, whereas the smallest spring environment is Billa Kalina Spring at 930 m^2. Tail environments where permanent surface water is found are generally densely vegetated, with the most common hydrophytes encountered being the reeds *Phragmites (sp. australis)* and *Typha* and the sedges and rushes *Cyperus, Baumera, Fimbristylis, Gahnia and Juncus* (Fatchen, 2001a; Holmes et al., 1981; Lange and Fatchen, 1990).

4.2.4 Geology of mound springs

In Chapter 3, tufa at these study sites is described as consisting of microbial, calcareous wackestone, grainstone or boundstone. Relict tufa distribution includes the mound structures and locally surrounding areas, however actively precipitating tufa was only found within current tail delta environments. Additionally, many features indicative of microbial influence, such as an abundance of oncoids and the development of thrombolitic textures are noted, as well as abundant reed castings and aquatic macrofaunal bioclasts. Prescott and Habermehl (2008) found ages of relict tufa material from still-active springs in the Lake Eyre South region of between 10,900 ±1,500 years and 740,000 ±120,000 years using thermoluminescence.

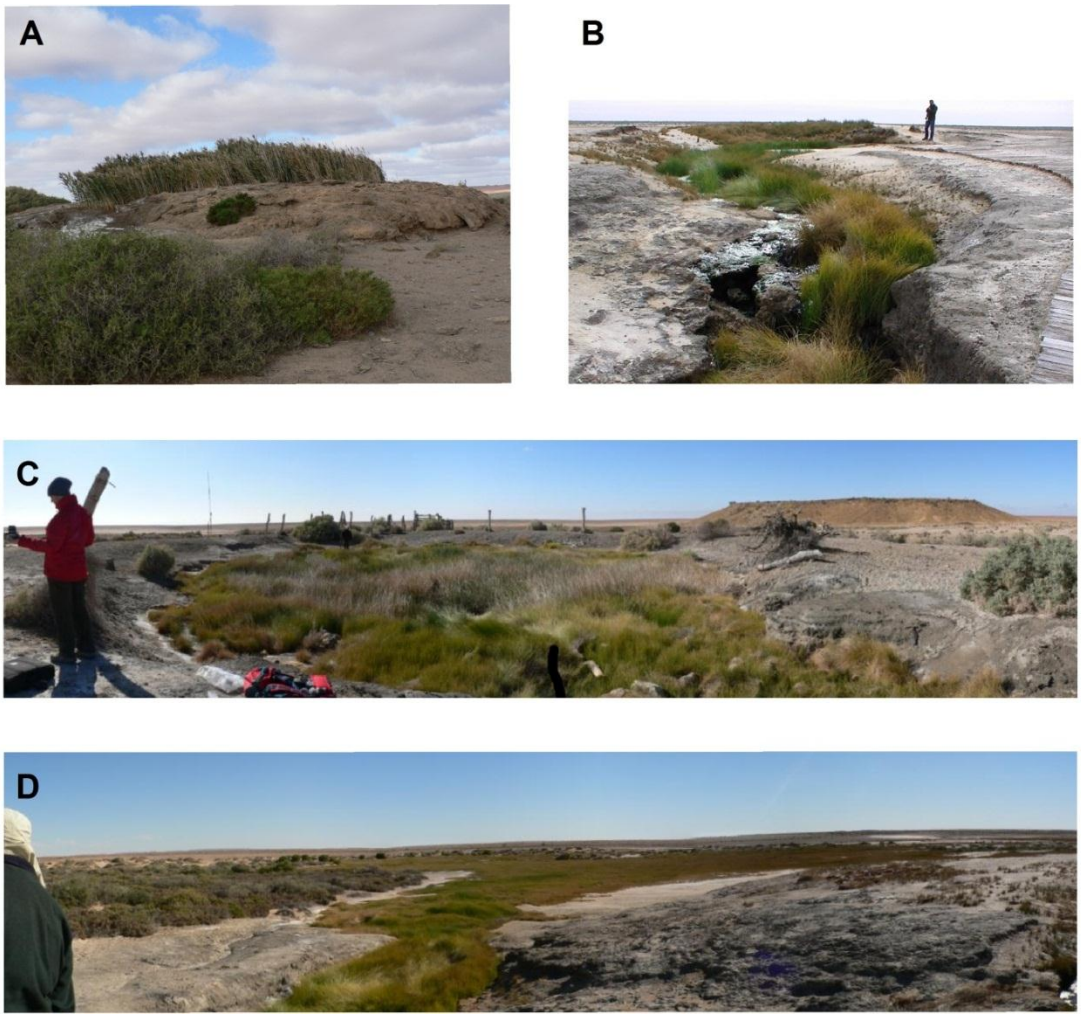

Figure 4.3: Morphological features of mound spring sites. A) The tufa mound spring at Billa Kalina Springs. Note the highly vegetated pool (predominantly phragmites) (a) and the bare tufa mound structure (b), which is a common feature of GAB tufa mound springs. B) A tail gutter or "break-out" at The Bubbler, with the spring pool near the top of the photograph (a). The small waterfall that developed within the tail gutter (b) is seen near the centre of the photograph. C) Composite photograph of the spring pool at Warburton Spring. Vegetation is largely floating on pool surface. D) Composite photograph of the tail delta at The Bubbler. The mound structure (a) can be seen in the bottom right hand corner of the photograph.

The unconsolidated sediments from the pool environments are described in Chapter 3 as predominantly composed of siliciclastic detrital sand and silt. Where the pool is vegetated, sediments also contained between 8 and 16% organic matter, whereas $CaCO_3$ contents of the pool sediments vary between 1 and 30%.

4.3 Sampling and Analytical Methods

4.3.1 Field methods

Water sampling sites at each study area were selected both to provide an even coverage over the length of the wetland and also to target sites within the environment that may be reflective of important hydrochemical change (Table 4.1 and Figure 4.4). Samples were collected in March and June/July 2009 in order to determine if temporal variations were important in relation to the hydrochemistry of the spring and tail water. The water temperature difference near the end of each sampling traverse ranged from 8 to 10°C between the sampling periods. This range is considered close to the maximum range that can be expected based on seasonal air temperature fluctuations.

Billa Kalina Spring is unique amongst the study sites in that there is a bore approximately 25 m from the vent of the main spring that has a depth of 28.5 m. Therefore, hydrochemical conditions between the aquifer and the surface environment could be closely compared. Because The Bubbler is located within a national park and receives a high number of visitors, fieldwork here was restricted to a single round of water sampling.

Sampling was conducted moving upstream so as to minimise disturbance. Salinity and pH measurements were taken using an YSI^{TM} 650 MDS water quality meter, which was calibrated for pH using 4.0 and 7.0 pH calibration standards and TDS using a 1,000 mg/L standard.

Table 4.1: Brief site description for each sampling site.

Substrate	Latitude (S)	Longitude (E)	Distance from vent (m)[a]	Site Description
Warburton Spring				
WSL1	29° 16' 27.43"	136° 40' 16.90"	0	Centre of pool over vent.
WSL2	29° 16' 27.40"	136° 40' 16.57"	9	Northern edge of spring pool.
WSL3	29° 16' 27.79"	136° 40' 16.43"	22	Tail gutter. 5m from edge of pool.
WSL4	29° 16' 28.62"	136° 40' 15.33"	61	Bottom of tail gutter. Dense sedge grass growth.
WSL5	29° 16' 29.44"	136° 40' 14.90"	88	Top of tail delta. Dense sedge grass growth.
WSL6	29° 16' 29.90"	136° 40' 13.87"	120	Upper tail delta. Dense sedge grass growth.
WSL7	29° 16' 30.66"	136° 40' 13.18"	150	Lower Tail delta, Oncoidal mud flats.
WSL8	29° 16' 31.70"	136° 40' 12.97"	182	Lower Tail delta, Oncoidal mud flats.
Billa Kalina Spring				
MSL1	29° 27' 37.77"	136° 29' 38.39"	0	Centre of pool over vent.
MSL2	29° 27' 37.58"	136° 29' 38.20"	8	Northern edge of spring pool.
MSL3	29° 27' 37.51"	136° 29' 38.12"	11	Tail gutter. Under small waterfall.
MSL4	29° 27' 37.42"	136° 29' 37.79"	19	Top of tail delta. Dense sedge grass growth.
MSL5	29° 27' 37.29"	136° 29' 37.56"	27	Tail delta. Oncoidal mud flats.
MSL6	29° 27' 37.20"	136° 29' 37.12"	38	Tail delta. Oncoidal mud flats.
The Bubbler				
BSL1	29° 26' 46.78"	136° 51' 28.80"	0	Centre of pool over vent.
BSL2	29° 26' 46.88"	136° 51' 28.62"	8	Tail gutter. 2.5m from edge of pool.
BSL3	29° 26' 47.09"	136°51' 28.48"	17	Tail gutter. Before small waterfall.
BSL4	29° 26' 47.33"	136° 51' 28.53"	26	Tail gutter. Base of small waterfall.
BSL5	29° 26' 47.41"	136°51' 27.78"	46	Bottom of tail gutter/ top of tail delta.
BSL6	29° 26' 46.47"	136° 51' 26.55"	90	Upper tail delta, Oncoidal mud flats.
BSL7	29° 26' 46.08"	136°51' 24.65"	144	Lower tail delta, Oncoidal mud flats.
BSL8	29° 26' 47.14"	136° 51' 23.37"	191	Lower tail delta, Oncoidal mud flats.

[a] Distance measured following thalweg.

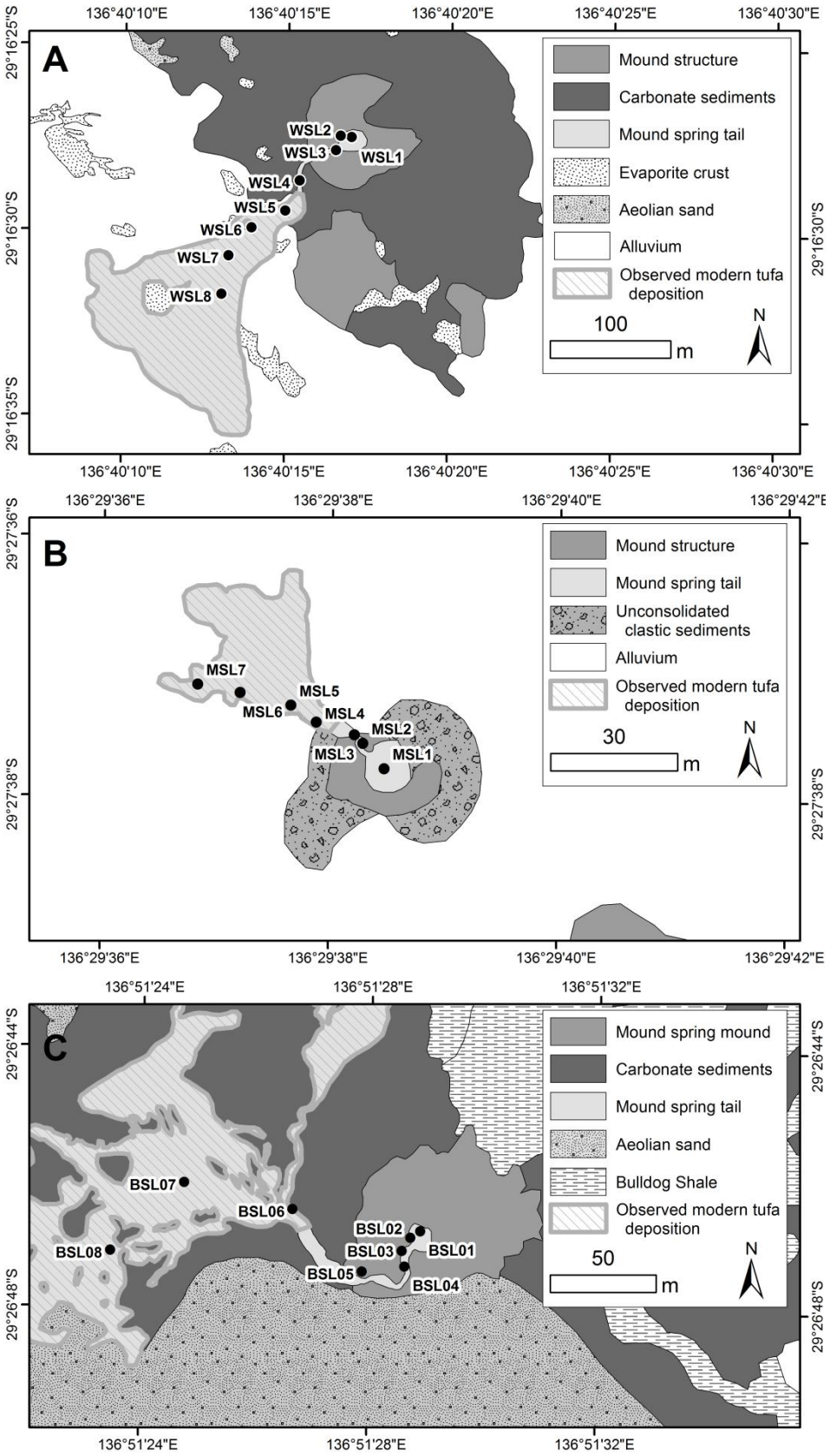

Figure 4.4: Water sampling localities at the various spring sites. A) Warburton Spring, B) Billa Kalina Spring and C) The Bubbler.

Calibration was undertaken before each spring site was sampled. In the cases of Warburton and Billa Kalina Springs, sampling traverses were limited to that part of the wetland where there was sufficient free standing surface water to collect a sample; areas further downstream were generally characterised by saturated soil conditions but little surface water. Alkalinity was measured in the field using a Hach^{TM} portable digital titration kit using a Bromcresol green-Methyl Red indicator. Samples were filtered using 0.45 μm filter paper to prevent any influence of carbonate on the titration.

Water from the site was collected using a plastic syringe that had been rinsed with distilled and sample-site water before collection. Sample water was then filtered over a 0.45 μm filter paper and collected and sealed in acid-washed 125 ml polyethylene (PE) plastic bottles. Samples designated for cation analysis were acidified with a few drops of 1M hydrochloric acid. Given that the δD and $\delta^{18}O$ values of water are sensitive to evaporation (Amundson and Kelly, 1987; Yoshimura et al., 2004) a glass 50 ml McCartney jar was filled with unfiltered sample water and sealed for stable isotope analysis.

All water analyses were completed at the CSIRO Land and Water analytical laboratories, Adelaide. DFW provided major ions and stable isotope data for samples collected in October 2008 from bores located in the vicinity of Warburton and Billa Kalina Springs. These data were used to compare hydrochemical conditions within the aquifer to those within the spring environment. SI_c and PCO_2 were calculated using the hydrochemical modelling code PHREEQC-2 (Parkhurst and Appelo, 1999) and the WATEQ4F hydrochemical database (Truesdell and Jones, 1974).

4.3.2 Water sample data processing

4.3.2.1 Chloride mass balance

The percentage of water lost to evapotranspiration was estimated using a Cl^- mass balance, which was calculated using:

$$F_{ET} = (1 - C_I / C_S) \cdot 100 \quad (1)$$

Where F_{ET} is the percentage of springwater lost to evapotranspiration, C_I and C_S are Cl^- (mg/L) in the input water and the sample, respectively. The Cl^- concentrations are not thought to be affected by cyclic precipitation and re-dissolution of salts, as the results showed that the strongest increase in dissolved Cl^- along the transect occurred during summer, i.e., the time of year in which salt precipitation is more likely, which would result in a reduction of the concentrations.

4.3.2.2 Stable isotope mass balance

The measured $\delta^{18}O$ values were used to estimate evaporation. A similar methodology was applied to δD data and similar results were obtained, therefore, these are not discussed for reasons of brevity. During evaporation, the lighter ^{16}O requires less kinetic energy to convert from the liquid to the gas phase, leaving the remaining water enriched with the heavier ^{18}O isotope. The transfer of water to the atmosphere by transpiration does not affect the isotopic composition of the remaining water (Gat, 1996); this is because water uptake by plant roots does not cause fractionation. Consequently any fractionation of stable isotopes observed can directly be attributed to evaporation. The ratio between water lost as evaporation (*E*) and inflow (*I*) can be expressed as follows (Craig and Gordon, 1965):

$$\frac{E}{I} = \frac{\delta_I - \delta_S}{\delta_E - \delta_S} \quad (2)$$

Where δ_I is the $\delta^{18}O$ value in the inflow water, δ_S is $\delta^{18}O$ value in the sample water and δ_E is the $\delta^{18}O$ value in the water vapour, with all $\delta^{18}O$ values in ‰ V-SMOW. Given the great difficulty involved with determining δ_E directly, this is generally calculated using a linear resistance model first developed by Craig and Gordon (1965).

$$\delta_E = \frac{\delta_L(1+10^{-3}\varepsilon^*) - h\delta_A - \varepsilon^* - \varepsilon_K}{1-h+10^{-3}\varepsilon_K} \quad (3)$$

Where, h is atmospheric relative humidity (between 0 and 1), δ_A is the isotopic composition of ambient moisture and ε^* is the equilibrium fractionation factor which was determined for ^{18}O using the empirically derived regression equation from Horita and Wesolowski (1994):

$$\varepsilon^*(‰) = -7.685 + 6.7123\left(\frac{10^3}{T}\right) - 1.6664\left(\frac{10^6}{T^2}\right) + 0.35041\left(\frac{10^9}{T^3}\right) \quad (4)$$

The value T is the interface temperature and ε_K (‰) in equation (3) is representative of the kinetic component of fractionation that can be determined using the relationship developed by Giofiantini (1986):

$$\varepsilon_k = C_k(1-h) \quad (5)$$

Where C_k is an experimentally derived constant, determined to be 14.2 ‰ for ^{18}O.

For March, relative humidity was estimated at h = 39% and for July at h = 25% (BoM., 2010). The value of δ_A was taken from Hamilton et al. (2005), who obtained δ_A = -17.7‰ for ^{18}O in the vicinity of Cooper Creek (central Australia) by sampling water from an evaporation pan using the method outlined in Gibson et al. (1999).

The values of C_I in equation (1) and δ_I in equation (2) were based on the water sample collected directly over the spring vent. The values for the water in the tail were always based on the sample collected furthest away from the vent.

4.3.2.3 Carbonate-reaction modelling

A hydrochemical transport model was developed to put quantitative constraints on the carbonate precipitation processes in the tail delta. The section between the vent and the end of the breakout is not considered in the model (Figure 4.5) as no carbonate precipitation is apparent from the field observations. The geometry of the delta-shaped tail was approximated by a sixth of a circle. For The Bubbler, the assumptions about the flow geometry were considered inappropriate due to the irregular shape of its tail environment and geochemical modelling was therefore not attempted for this spring. The flow conditions were assumed to be in steady state, with inflow from the spring vent Q (L^3/T) being equal to the total amount of water lost via evapotranspiration (ET) and infiltration (In) over the extent of the tail (i.e., $Q = ET+In$).

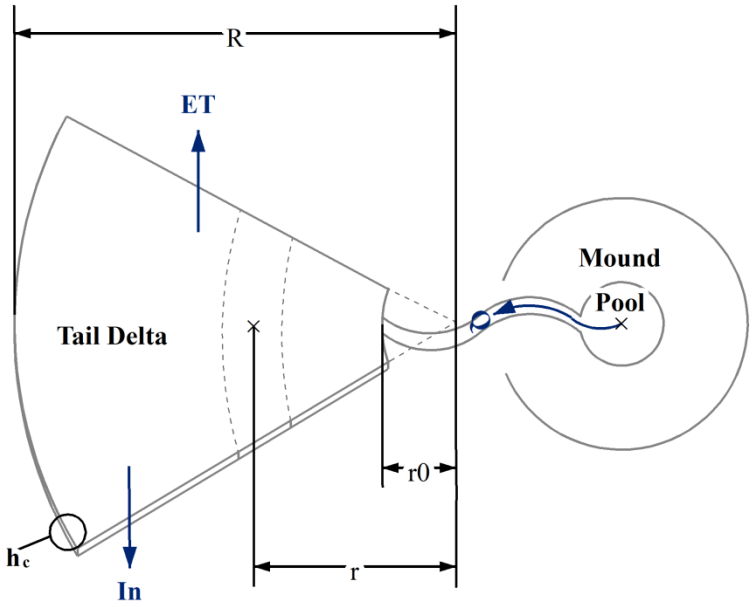

Figure 4.5: Graphical representation of the geometry-based hydrochemistry model used to simulate $CaCO_3$ precipitation within the tail delta environment. *R* is the maximum length the delta can reach, *r* is the distance to a designated cell area, *r0* is that part of the circle fraction not included within the model, *Q* is the initial water flow into the model, *E* and *I* are water loss through evaporation and infiltration respectively and h_c is the height of the water column.

If it is assumed that the evapotranspiration flux *e* (L/T) and infiltration flux *i* (L/T) are spatially uniform and constant in time, the theoretical steady-state radius of the tail is:

$$R = \sqrt{\left(\frac{Q}{\alpha}\right) + r_0^2} \qquad (6)$$

Where *R* is the maximum radius of the tail environment (L), r_0 is the radius of the inner part of the circle not included in the model (L) and $\alpha = \pi(e+i)/6$ (L/T).

PHREEQC-2 uses a mixing-cell approach to simulate transport along a flow-line with a constant residence time in each cell (Parkhurst and Appelo, 1999). In the

radial flow situation considered, the flow velocity will progressively decrease towards the tail rim as the flow area widens and more water is lost by evapotranspiration and infiltration. For the idealised flow conditions considered here, this can be expressed as:

$$v(r) = \frac{Q-\alpha(r^2-{r_0}^2)}{\beta r} \quad (7)$$

Where v is the flow velocity (m/day), $\beta = 2\pi h_c/6$ and h_c is the height (m) of the water column, which is assumed to be constant throughout the tail. With the residence time in each cell being constant, the cell length decreases progressively. Cell lengths can be found by noting that $v(r)=dr/dt$. Rewriting equation (7) and integrating equation (8):

$$\int_{t_n}^{t_{n+1}} dt = \int_{r_n}^{r_{n+1}} \frac{\beta r}{Q-\alpha(r^2+{r_0}^2)} dr \quad (8)$$

Yields:

$$t_{n+1} - t_n = \frac{\beta ln(Q+\alpha{r_0}^2-\alpha{r_n}^2)}{2\alpha} - \frac{\beta ln(Q+\alpha{r_0}^2-\alpha{r_{n+1}}^2)}{2\alpha} \quad (9)$$

Substituting σ for $Q+{r_0}^2$ and solving for r_{n+1} gives:

$$r_{n+1} = \sqrt{\frac{\sigma-(\sigma-\alpha{r_n}^2)\exp(\frac{2\alpha}{\beta}(t_n-t_{n+1}))}{\alpha}} \quad (10)$$

By assigning a radial distance (r_1) for the first cell and by defining a fixed time step $t_n - t_{n+1}$, equation (10) can then be used to calculate the lengths of the consecutive cells.

Total water loss rates, i.e., $e + i$, from the wetland were calculated based upon the methodology developed by Williams and Holmes (1978) and are provided in Table 4.2. This method is based upon the ratio between measured discharge (m^3/day) from a spring and the area of the resulting wetland (m^2). Wetland area was based upon aerial photographic interpretation. Discharge rates were obtained from salt dilution tests completed in October 2008 (Halihan pers. comm., 2008) or from temporary weir measurement by BHP Billiton (2005).

For Warburton Spring, sample sites 4 to 8 (Figure 4.4A) and for Billa Kalina Spring sample sites 3 to 6 (Figure 4.4B) were assessed by the model. The initial water hydrochemistry conditions entered into the model were sample 4 and sample 3 (Figure 4.4) for Warburton and Billa Kalina Spring, respectively.

Table 4.2: Constants used in carbonate hydrochemistry modelling.

Constant	Warburton Spring March 2009	Warburton Spring June 2009	Billa Kalina Spring March 2009	Billa Kalina Spring June 2009
Area of Wetland (m^2)	16,000	16,000	930	930
Radius of first cell (m)	40	40	15	15
Discharge (m^3/day)	259	259	26	26
Total water loss (mm/day)	16	16	18	18
ET water loss rate (mol/sec)	1.7×10^{-4}	2.5×10^{-5}	3.5×10^{-4}	1.0×10^{-6}
Height water column (h_c) (m)	0.02	0.02	0.15	0.15
No Cells	15	15	30	30
Time step (s)	8640	8640	2160	2160
Gas ex. rate con. CO_2 *k* (/sec)	7.5×10^{-4}	3.5×10^{-4}	-8.5×10^{-4}	-3.0×10^{-4}
Heterotrophic CO_2 add. rate (cells) (mol/sec)	1.1×10^{-8} (7-15)	$1.1. \times 10^{-8}$ (4-15)	2.6×10^{-8} (7-30)	2.6×10^{-8} (5-30)

The chemical processes that were considered were kinetically-controlled calcite precipitation, CO_2 degassing and CO_2 production via net heterotrophy. Calcite precipitation was modelled using the kinetic rate equation built into the WATEQ4F database employed by PHREEQC-2 as developed by Plummer et al. (1978). The loss of CO_2 to atmosphere was described using the rate expression from Bennett and Rathbun (1972):

$$rc_T = k(CO_2 - CO_{2(eq)}) \quad (11)$$

Where rc_T (mol/sec) is the reaction term for CO_2 transfer from water to atmosphere, *k* (/sec) is the gas exchange rate constant, CO_2 (mol) is the actual CO_2 concentration and $CO_{2(eq)}$ (mol) is the CO_2 concentration in water, when CO_2 exchange between air and water is at equilibrium. The value of *k* was optimised to match observed PCO_2.

This parameter integrates a number of influences on degassing that are difficult to quantify, including the substrate surface area contact of water as a proportion of volume, perturbation caused by micro-turbulence and any effect biota may be having on degassing, either chemically or physically. The most accurate determinations of the gas exchange rate constant *k* are estimated using a tracer experiment, where a conservative gas such as propane is injected into the stream reach under consideration (Tsivoglou et al., 1965). As it was not possible to conduct such an experiment during the course of this study, the optimised *k* values used were compared to published values (Choi et al., 1998; Genereux and Hemond, 1992; Longsworth, 1991). Although there are recognised morphological differences between the streams of previously published work and the environments presented here, the similarity between the values that were obtained after model optimisation (as discussed below) is encouraging.

Net heterotrophic metabolism associated with the generation of CO_2 is a common feature of wetland environments and has been studied in relation to aquatic health (Neal et al., 2002; Stratford et al., 2004) and potential contribution to atmospheric CO_2 (e.g. Couwenberg et al., 2010; Seo and DeLaune, 2010). Heterotrophy is normally assumed to be caused by decomposition of organic matter that is accomplished via a number of processes including: a) aerobic respiration by microorganisms, b) anaerobic respiration, fermentation and methanogenesis by bacteria, and/or c) aerobic or anaerobic metabolism by macrophytes. These processes involve the consumption of oxygen, with oxygen sourced from either dissolved concentrations or from the stems of plants (Hamilton et al., 1995). The observed consumption of dissolved oxygen (DO) in the lower tail environments from field

measurements suggested that net heterotrophy may be occurring where spring wetland waters were most dispersed and stagnant (Table 4.3). Net heterotrophy was replicated by the addition of CO_2 to the model to cells representative of the downstream part of the wetland environment using a zero-order rate expression. The rate constants are listed in Table 4.2.

Evapotranspiration rates were calculated using Cl^- and considered in the model by removing water at the rates shown in Table 4.2. The transport algorithm of PHREEQC-2 simulates advective transport by transferring the solution from each model cell to the next cell after each time step (Parkhurst and Appelo, 1999). The decreasing velocity towards the downstream end of the tail delta was simulated by decreasing the cell length in accordance with equation (10). Diffusive mixing was taken into account by specifying a diffusion coefficient of 10^{-9} m^2/sec. This description of the transport processes was considered appropriate for the quiescent flow conditions in the tail delta, where the flow can be considered to be laminar rather than turbulent.

4.4 Results

A table of water quality measurements and chemistry analyses collected from each of the bore and spring localities can be found in Table 4.3.

4.4.1 Water chemistry

4.4.1.1 Warburton Spring

Warburton Spring has a discharge rate of approximately 3.0 L/sec (Halihan pers. comm., 2008) and modern tufa accumulation was evident in areas downstream of site 4 (Chapter 3). Graphs of key water quality measurements and hydrochemistry results can be found in Figure 4.6. The spatial variation of pH was very similar between the data sets, displaying a gradual change from near neutral conditions at the pool centre (site 1) to alkaline conditions within the tail gutter (site 3), followed by a further increase between the tail gutter and the lower tail delta.

Alkalinity remained stable between the spring vent and site 6, ranging between 500 and 620 mg/L (expressed as $CaCO_3$). A decrease in alkalinity occurred in both data sets downstream of sample 6. The distribution of Ca^{2+} along the traverse is similar to alkalinity: Ca^{2+} remained relatively constant until a point downstream of site 6, after which point Ca^{2+} declined rapidly. In addition, a small but significant increase in Ca^{2+} between the pool centre (site 1) and the upper tail (site 3) was also observed.

The calculated SI_c indicated a change from near-equilibrium to over-saturation from the pool centre (site 1) to the upper tail (site 3). A rapid increase in SI_c to above 1 was recorded from site 4 onwards. The calculated values for SI_c for March were approximately 0.3 higher than those for June.

Table 4.3: Major ion, stable isotope, PCO_2 and SI_c results for water samples from Warburton Spring, Billa Kalina Spring and The Bubbler.

Sample Station	Date	Dist. (m)	pH	EC (mS/cm)	T °C	Alk.[a] (mg/L)	DO (mg/L)	Ca^{2+} (mg/L)	Mg^{2+} (mg/L)	Na^{+} (mg/L)	K^{+} (mg/L)	Si^{2+} (mg/L)	Sr^{2+} (mg/L)	Cl^{-} (mg/L)	Br^{-} (mg/L)	SO_4^{2} (mg/L)	$\delta^{18}O$ (‰)	δD (‰)	PCO_2 (matm)	SI_C	CBE (%)
Warburton Spring																					
6239-4	Oct-08	4094	6.77	7.12	28.1	770	1.02	74.1	35.3	1265	44.8	7.0	2.6	1528	1.4	252	-7.02	-45.3	142.0	-0.11	-0.68
WSL1	Mar-09	0	7.06	6.05	27.3	546	0.53	80.1	38.4	1356	43.3	8.1	2.7	1470	1.6	277	-6.74	-46.7	50.8	0.05	7.35
WSL2	Mar-09	9	7.54	6.68	24.8	534	6.37	82.1	38.9	1372	44.4	8.7	2.7	1530	1.5	274	-6.62	-45.6	15.7	0.50	6.74
WSL3	Mar-09	22	7.46	6.61	27.1	526	5.55	83.6	40.0	1391	44.9	9.0	2.8	1504	1.5	265	-6.73	-45.6	19.2	0.45	8.40
WSL4	Mar-09	61	8.21	6.60	26.1	530	8.51	78.6	39.7	1379	44.8	8.9	2.8	1515	1.6	268	-6.58	-45.4	3.2	1.13	7.47
WSL5	Mar-09	88	8.24	6.61	26.1	516	7.68	82.4	40.2	1398	45.0	8.9	2.8	1502	1.6	266	-6.65	-45.6	2.9	1.16	8.79
WSL6	Mar-09	120	8.31	6.67	23.4	516	10.15	79.9	40.7	1423	47.0	9.0	2.8	1561	1.6	278	-6.49	-44.5	2.4	1.18	7.96
WSL7	Mar-09	150	8.56	7.12	24.8	464	9.02	51.8	39.4	1633	48.0	8.8	2.5	1815	1.9	337	-6.09	-41.3	1.2	1.17	7.38
WSL8	Mar-09	182	8.62	7.80	24.7	460	5.31	39.9	38.1	1676	47.9	8.4	2.4	1880	1.9	360	-5.28	-39.4	1.0	1.09	6.48
WSL1	Jun-09	0	7.03	5.21	27.6	589	0.27	75.6	41.3	1340	47.5	6.6	2.6	1580	3.8	290	-6.76	-43.6	58.9	0.03	3.20
WSL2	Jun-09	9	7.32	6.03	21.3	584	4.1	78.7	41.6	1350	48.3	6.7	2.7	1616	3.9	313	-6.76	-43.5	27.3	0.24	2.57
WSL3	Jun-09	22	7.41	6.71	24.8	572	4.04	78.2	41.2	1330	47.8	6.7	2.7	1584	3.8	288	-6.90	-44.0	22.8	0.37	3.20
WSL4	Jun-09	61	8.03	6.70	23.3	601	8.24	78.3	41.5	1340	48.0	6.8	2.7	1613	3.9	295	-6.71	-44.6	5.5	0.97	2.32
WSL5	Jun-09	88	8.13	6.50	22.6	573	7.75	77.2	41.7	1340	47.9	6.8	2.6	1598	3.8	292	-6.69	-44.4	4.1	1.03	3.14
WSL6	Jun-09	120	8.20	6.72	20.3	572	11.7	75.9	42.0	1370	48.4	6.9	2.7	1603	3.8	293	-6.66	-45.7	3.3	1.06	3.99
WSL7	Jun-09	150	8.20	6.70	18.0	502	9.6	52.0	41.3	1380	49.4	6.9	2.4	1636	2.3	300	-6.49	-44.2	2.9	0.82	3.67
WSL8	Jun-09	182	8.31	6.79	19.0	488	11.6	38.7	38.4	1400	49.8	6.8	2.2	1681	4.1	308	-6.16	-42.0	2.2	0.79	2.70

[a]Alkalinity reported as $CaCO_3$

Table 4.3: Major ion, stable isotope, PCO_2 and SI_c results for water samples from Warburton Spring, Billa Kalina Spring and The Bubbler (cont.).

Sample Station	Date	Dist. (m)	pH	EC (mS/cm)	T °C	Alk.[a] (mg/L)	DO (mg/L)	Ca^{2+} (mg/L)	Mg^{2+} (mg/L)	Na^{+} (mg/L)	K^{+} (mg/L)	Si^{2+} (mg/L)	Sr^{2+} (mg/L)	Cl^{-} (mg/L)	Br^{-} (mg/L)	SO_4^{2} (mg/L)	$\delta^{18}O$ (‰)	δD (‰)	PCO_2 (matm)	SI_C	CBE (%)
Billa Kalina Spring																					
6139-22	Oct-08	27	6.08	8.75	24.2	595	5.54	126.6	28.7	1620	50.9	5.0	3.2	2189	2.2	362	-6.82	-44.2	496.6	-0.77	-0.34
MSL1	Mar-09	0	6.88	7.88	23.9	416	1.02	152.6	30.4	1745	55.7	5.5	4.2	2134	2.3	379	-6.73	-45.9	54.3	-0.05	6.89
MSL2	Mar-09	8	7.36	9.16	19.7	420	3.07	162.3	33.1	1916	59.4	4.0	4.5	2284	2.5	395	-6.53	-44.8	16.9	0.39	8.46
MSL3	Mar-09	11	7.75	9.04	20.1	412	7.96	156.4	32.3	1861	58.0	4.8	4.5	2247	2.5	380	-6.72	-44.3	6.7	0.76	7.92
MSL4	Mar-09	19	8.06	9.10	18.5	384	9.73	147.8	33.9	1961	61.5	4.6	4.5	2271	2.5	387	-6.45	-44.2	2.9	0.98	9.96
MSL5	Mar-09	27	8.27	9.95	21.3	308	11.27	111.0	33.8	1740	56.9	3.9	3.9	2272	2.5	387	-6.44	-45.3	1.5	1.01	4.47
MSL6	Mar-09	38	8.11	11.36	23.9	366	7.12	121.0	45.1	2330	77.0	5.8	5.0	3189	3.1	565	-4.85	-37.0	2.6	0.94	1.88
MSL1	Jun-09	0	7.08	9.13	16.7	602	2.9	201.0	41.5	2100	79.5	9.7	5.3	2825	6.4	466	-6.47	-43.0	43.9	0.29	2.56
MSL3	Jun-09	11	7.18	4.76	18.7	492	0.05	150.0	34.6	1890	63.4	5.2	4.3	2551	5.8	406	-6.61	-44.4	29.7	0.23	2.13
MSL4	Jun-09	19	8.03	9.06	17.9	492	13.14	137.0	34.4	1890	64.3	5.0	4.3	2584	5.7	424	-6.38	-43.2	4.0	1.01	1.06
MSL6	Jun-09	38	7.84	6.89	16.6	324	10.39	97.7	31.0	1900	62.8	4.2	3.7	2504	5.5	431	-6.15	-40.8	4.1	0.49	3.15
The Bubbler																					
BBL1	Jul-09	0	7.15	2.46	30.4	814	0.34	36.7	28.3	1160	32.7	6.1	1.4	1204	2.8	127	-6.84	-47.9	66.1	0.05	2.37
BBL2	Jul-09	8	7.18	4.68	30.0	806	2.11	36.8	28.2	1150	32.4	5.9	1.4	1207	1.6	126	-6.93	-46.1	60.3	0.07	2.05
BBL3	Jul-09	17	7.14	4.91	29.8	760	2.55	36.0	28.1	1140	32.5	5.8	1.4	1215	2.9	128	-6.92	-43.7	61.7	0.00	2.13
BBL4	Jul-09	26	7.38	4.73	29.7	825	5.73	36.1	28.1	1140	32.6	5.8	1.3	1211	2.3	128	-6.84	-45.6	38.9	0.26	1.11
BBL5	Jul-09	46	7.49	4.67	29.7	810	12.14	35.8	28.1	1130	32.2	5.7	1.3	1211	3.0	127	-6.90	-45.3	29.5	0.36	0.88
BBL6	Jul-09	90	8.66	4.94	26.8	745	10.88	35.1	28.4	1150	32.7	5.9	1.4	1211	4.5	126	-6.82	-45.7	1.5	1.34	2.98
BBL7	Jul-09	144	8.31	4.96	24.8	820	7.63	31.0	28.4	1140	32.7	5.8	1.3	1247	2.3	131	-6.86	-44.7	4.0	1.01	-0.13
BBL8	Jul-09	191	8.90	4.75	21.9	748	13.86	26.6	27.8	1130	32.7	5.9	1.2	1240	2.9	130	-6.66	-44.2	0.8	1.36	0.78

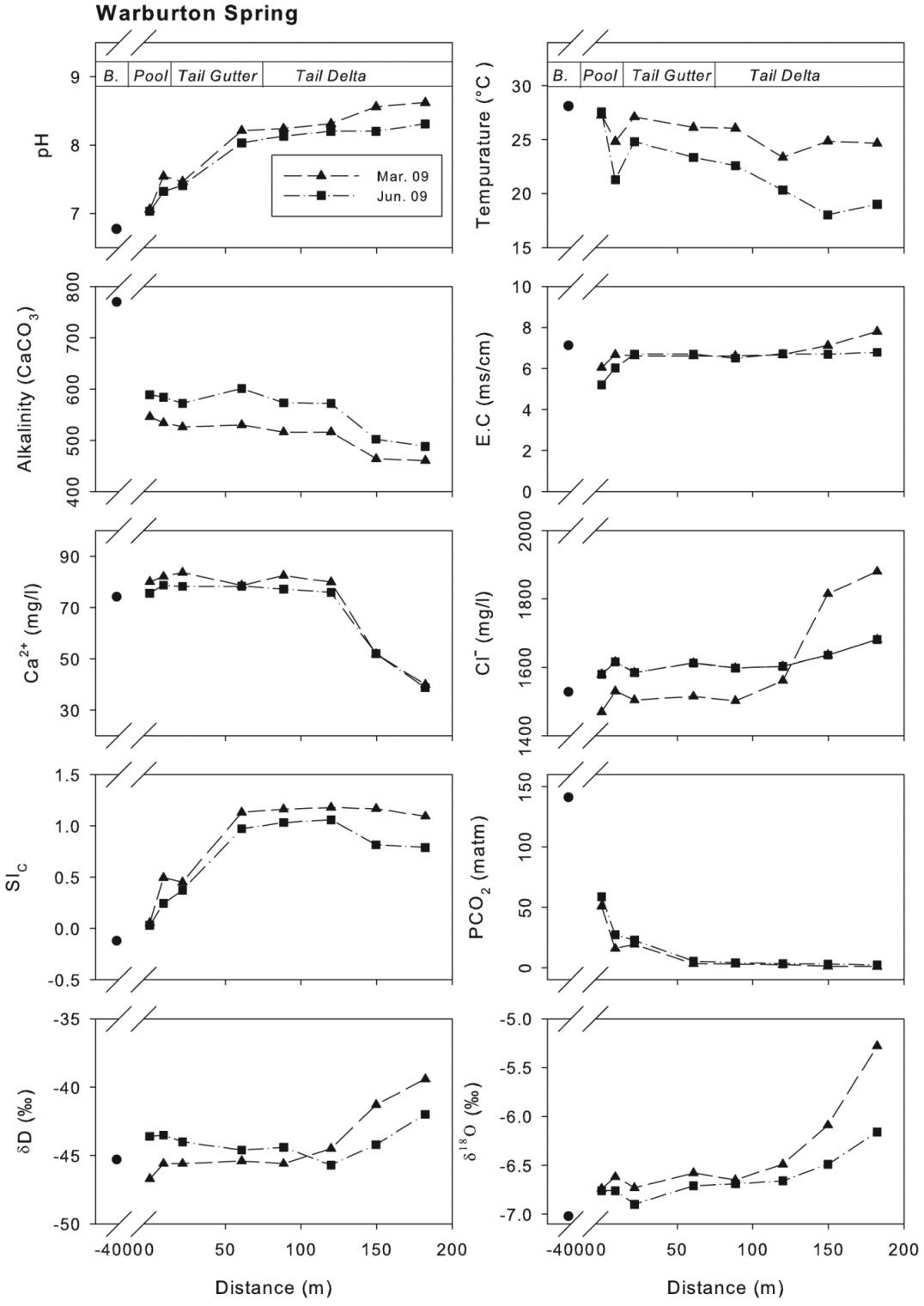

Figure 4.6: Graphs of key water quality measurements and hydrochemistry results, Warburton Spring. B.: Bore.

Calculated PCO_2 values indicated a rapid degassing occurred from springwater between the pool-centre to approximately the top of the tail delta (site 4) at which

point CO_2 degassing slowed considerably. The PCO_2 value of the well sample was almost 50% higher than the equivalent pool sample and approximately 4 orders of magnitude greater than the atmospheric partial pressure of approximately 4 matm.

Using Cl^- mass balance, a water loss by evapotranspiration of approximately 22% in March and 6% in June was estimated. The results from stable isotopes indicate that the evaporation component (based on $\delta^{18}O$) amounted to 6.4 % in March and 2.6 % in June. Most evaporation occurred within the lower tail environments, represented by the last 2 or 3 samples of each traverse, as can be seen from Figure 4.6. Finally, the change in water temperature indicates a trend towards thermal equilibrium with atmospheric temperature

4.4.1.2 Billa Kalina Spring

Billa Kalina Spring is the smallest spring system sampled during fieldwork, with a discharge rate of approximately 0.21 L/sec (Halihan pers. comm., 2008). The number of sampling sites varied from 6 to 4 (Figure 4.4). Modern tufa deposition was observed in the vicinity and downstream of site 4.

Graphs of water quality measurements can be found as Figure 4.7. The distribution of pH was very similar between the data sets, displaying a change from slightly acidic at the pool to alkaline conditions in the vicinity of sample 5 in the lower tail.

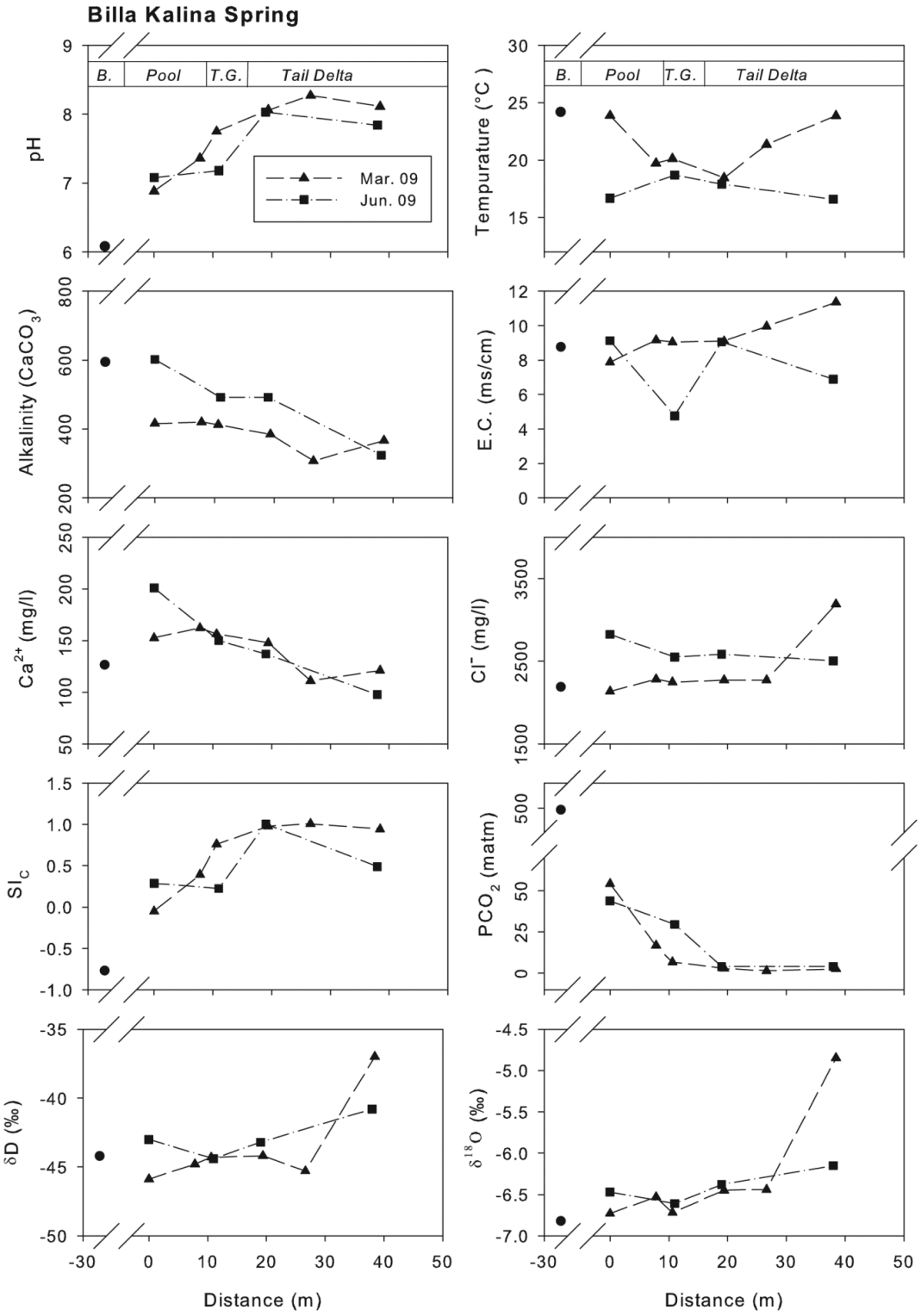

Figure 4.7: Graphs of key water quality measurements and hydrochemistry results, Billa Kalina Spring. B.: Bore. *T.G.*: Tail gutter.

Alkalinity generally decreased with distance from the spring vent and ranged between 602 and 308 mg/L (as $CaCO_3$). Ca^{2+} in the March data set increased modestly between the edge of the pool and the centre, followed by a gradual decrease down the tail, while the general trend displayed in the June data set was a decrease in concentration.

The calculated SI_c for both data sets showed a similar trend, with a steady increase from near saturated to over-saturated conditions. Calculated PCO_2 values exhibited a rapid decrease until site 4, where a near-constant concentration at or below 5 matm occurred. The PCO_2 value of the well sample was over three orders of magnitude greater than atmospheric PCO_2 and was approximately 5 times greater than the pool sample.

The central pool temperature for the June data set was low compared to March, which was attributed to difficulty experienced in the field in locating freshly emerged springwater due to the thickness of *phragmites* growth. It cannot be excluded that the concentration and isotope values measured in this sample were slightly higher than the actual springwater due to more stagnant conditions at the actual sampling site. Nevertheless, similarly to Warburton Spring, the change in water temperature indicated a trend towards equilibrium with atmospheric temperature. The δD and $\delta^{18}O$ values showed greater enrichment within the tail in March than in June.

Using Cl^- mass balance, a water loss of approximately 33% attributable to evapotranspiration was reported in March, while in comparison a water loss of 8.3% attributable to evaporation only was approximated using $\delta^{18}O$ mass balance. Very

little water loss was apparent by either evaporation or transpiration in June; approximately 1.3% of water loss could be attributable to evaporation, while evapotranspiration could not be determined using Cl^- from June samples.

4.4.1.3 The Bubbler

The Bubbler is the largest spring system sampled during fieldwork and is the largest spring by current discharge rate located within the Lake Eyre South region, with a discharge rate of approximately 10 L/sec (BHP Biliton, 2005). 8 sites from the spring vent to the lower reaches of the tail were sampled at The Bubbler (Figure 4.4), including sites located immediately before and within the splash zone of a waterfall that occurs approximately 20 m from the vent. Modern tufa appeared within the lower tail environment downstream of site 5. Graphs of water quality measurements can be found as Figure 4.8.

pH remained at near neutral conditions in the vicinity of the pool and the top of the tail gutter (sites 1-3) before changing to alkaline conditions at the top of the tail delta (site 6). A gradual decline in Ca^{2+} occurred from the spring vent to site 6; after this point, the decline in concentrations was more rapid. Calculated SI_c remained at a near-saturated level for the first three sites, and then gradually increased to 0.36 at site 4 and 5. Between sites 5 and 6, a large increase to over-saturation was observed, with samples all possessing a SI_c of greater than 1.

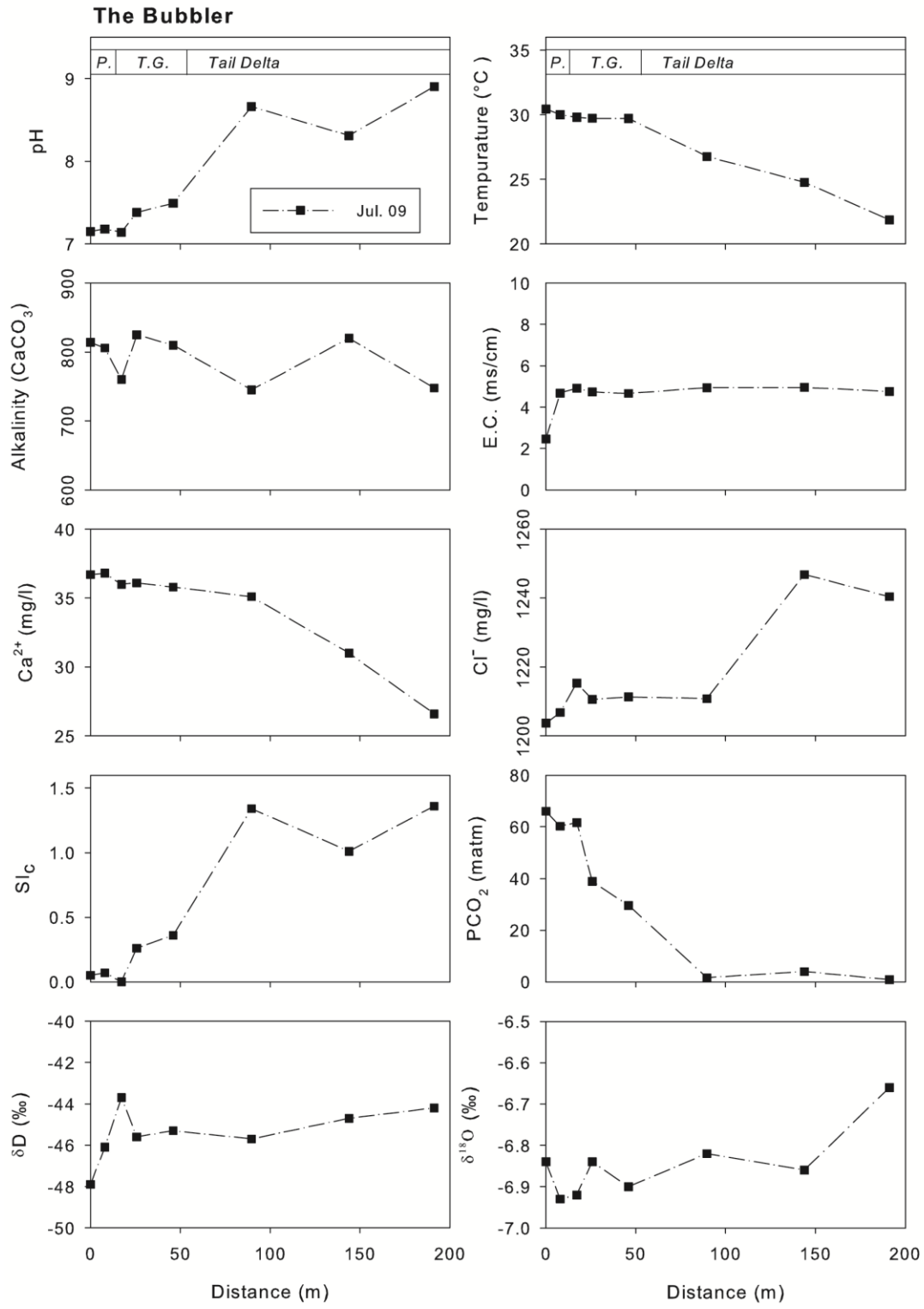

Figure 4.8: Graphs of key water quality measurements and hydrochemistry results, The Bubbler. P.: Pool. T.G.: Tail gutter.

Calculated PCO_2 values appeared relatively stable between 60 and 66 matm over the first three sites, located within the pool and the top of the tail gutter. Rapid degassing of CO_2 occurred between samples 3 and 4 within the most turbulent part of the tail gutter. CO_2 degassing slowed considerably by site 6, some 90 m from the spring vent and within the lower tail environment.

The change in water temperature reflected a trend towards thermal equilibrium with atmospheric temperature, which was approximately 23°C at the time of the survey. The δD, $\delta^{18}O$ and Cl^- results displayed a weak enrichment towards the end of the transect, although the observed changes are close to the analytical accuracy. Water loss by evapotranspiration (inferred from Cl^-) of approximately 3% was estimated whereas evaporative loss (inferred from $\delta^{18}O$) was 0.7%.

4.4.2 Carbonate hydrochemistry modelling

Results of modelling are presented as Figures 4.9 and 4.10 for Warburton and Billa Kalina Springs respectively. In each case, the employed hydrochemistry constants as described in Table 4.2 were optimised to provide the best fit however, Table 4.2 only displays the constant values used in the final model.

In the model, a value of e = 5.3 mm/day for Warburton Spring and e = 8.2 mm/day for Billa Kalina Spring for summer and 0.8 mm/day and 0.02 mm/day for winter have been used based on the Cl^- results.

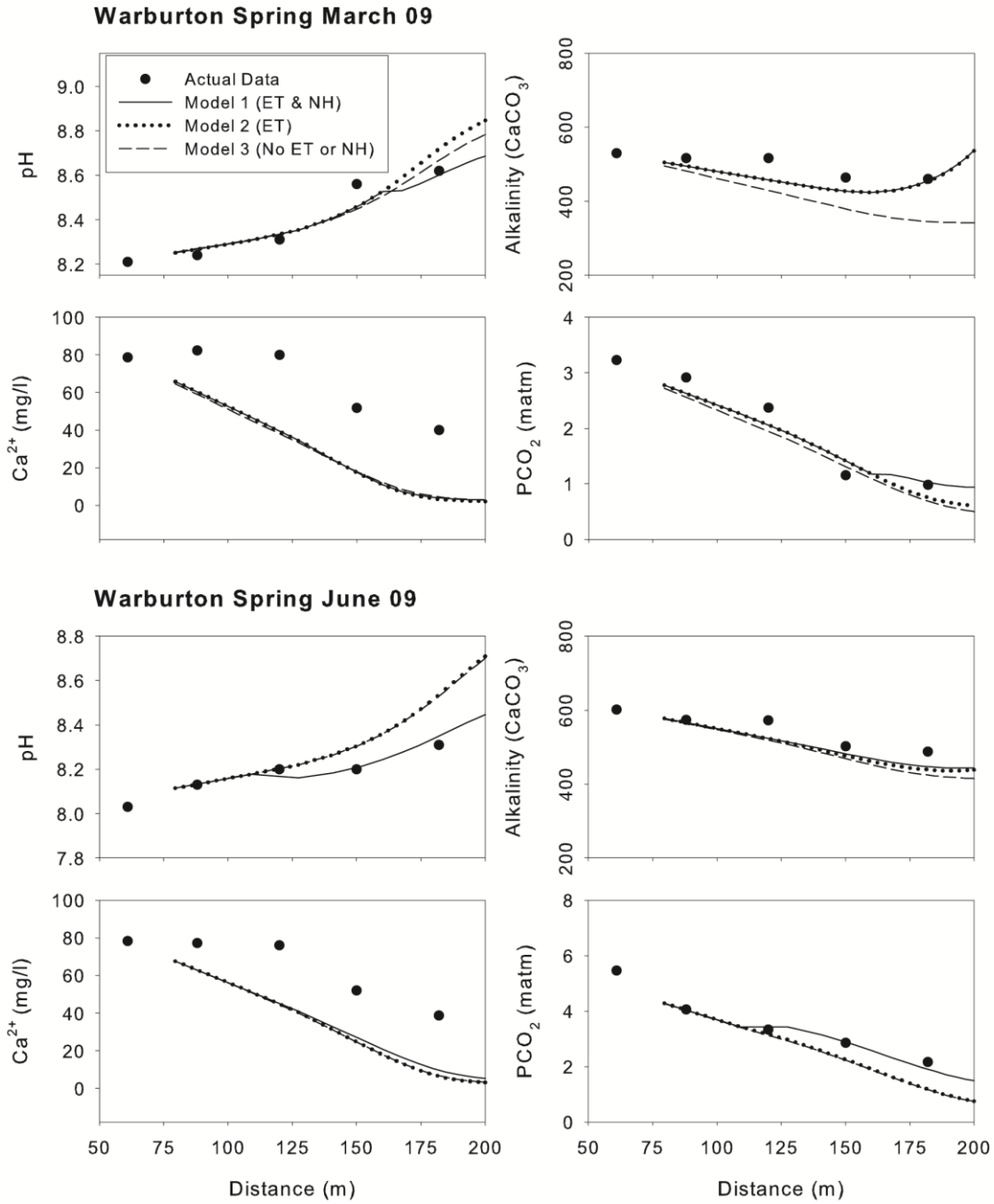

Figure 4.9: Modelled versus field data for tail delta environment, Warburton Spring. *ET*: Evapotranspiration. *NH*: Net Heterotrophy.

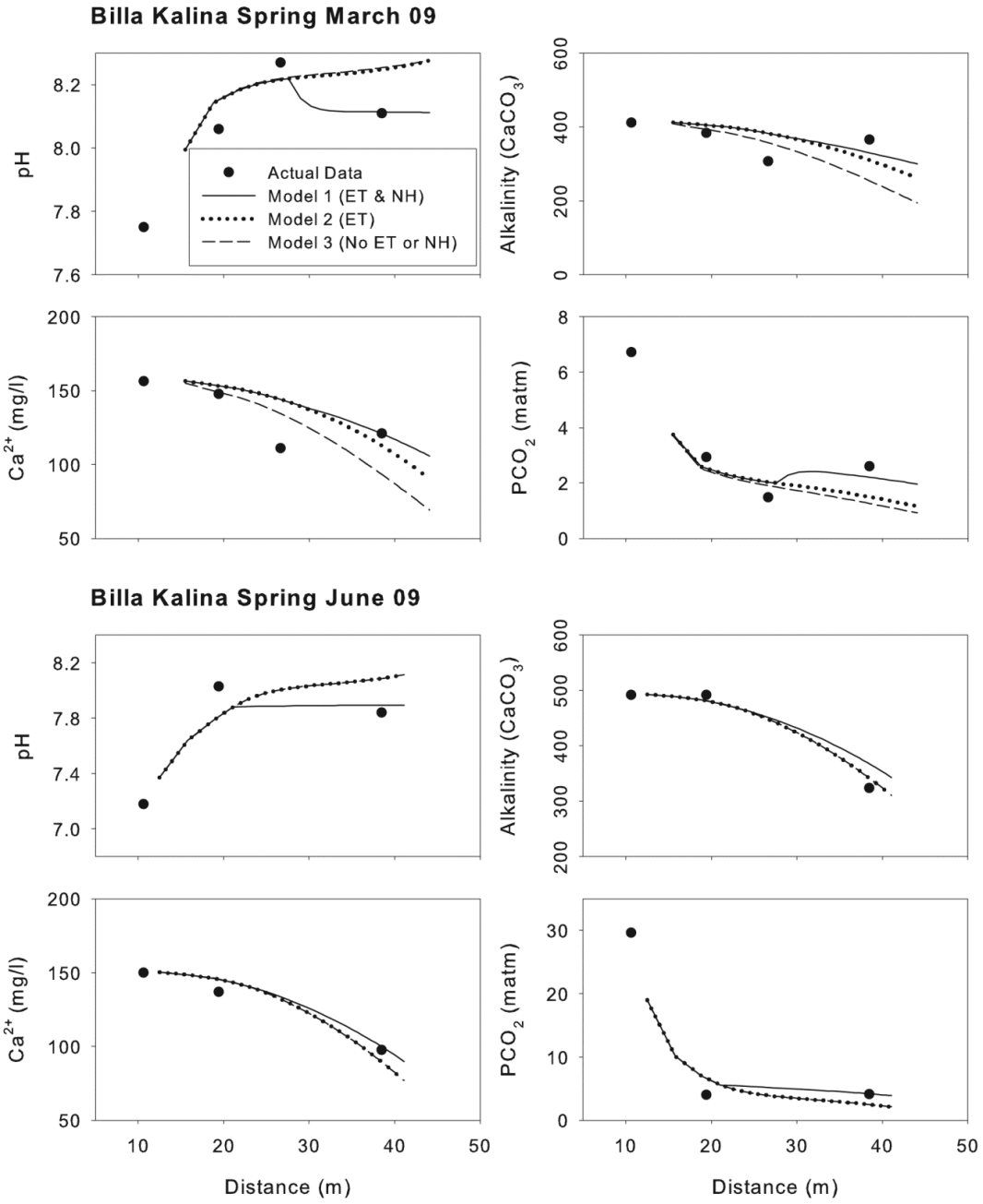

Figure 4.10: Modelled versus field data for tail delta environment, Billa Kalina Spring. *ET*: Evapotranspiration. *NH*: Net Heterotrophy.

This implies that for summer i = 10.7 mm/day for Warburton Spring and i = 9.8 mm/day for Billa Kalina Spring and in winter, i = 15.2 mm/day for Warburton Spring and i = 17.98 mm/day for Billa Kalina Spring.

For Warburton Spring, the reactive transport model is thought to adequately simulate the field data; the modelled PCO_2, alkalinity and pH in particular show good agreement. The modelled onset of calcite precipitation is earlier than observed in the field, although the rate of calcium (Ca^{2+}) removal appears adequate.

Similarly to Warburton Spring, the modelled data for Billa Kalina Spring are considered reasonably representative of field measurements. Unlike Warburton Spring, the apparent inhibition of calcite loss within the upper tail delta does not occur, resulting in a reasonable correlation between modelled and measured Ca^{2+} data.

In both cases, water loss via evapotranspiration appears to only have a small effect on hydrochemistry (Figure 4.9 and 4.10). In the case of Warburton Spring, removing evapotranspiration from the model most greatly affects alkalinity and pH, but only has a negligible effect on carbonate precipitation (Figure 4.9). At Billa Kalina Spring estimated water loss is not significant enough to impart any meaningful influence on the modelled outcome (Figure 4.10).

Likewise, CO_2 invasion into wetland waters in the lower tail as a consequence of interpreted net heterotrophy has a small but notable effect on the modelled outcome of pH and PCO_2 values (Figures 4.9 and 4.10). The addition of such CO_2 to the model improves the modelled fit of these two quantities compared to the model in

which it is excluded, although it does not have a significant influence on $CaCO_3$ precipitation.

4.5 Discussion

According to Buhmann and Dreybrodt (1985), the chemical processes that control the kinetics of $CaCO_3$ precipitation include (i) diffusive transport of the dissolved species, i.e. Ca^{2+}, HCO_3^-, CO_3^{2-}, CO_2 and H_2CO_3 to the liquid/ solid phase boundary, (ii) the kinetics of the conversion of carbonic acid (H_2CO_3) to CO_2 gas and (iii) the kinetics of precipitation at the phase boundary between the aqueous solvent and the substrate surface.

Of these steps, the conversion of H_2CO_3 to CO_2 gas is the slowest and is therefore the rate-limiting step for $CaCO_3$ precipitation from solution. Environments that are conducive for $CaCO_3$ precipitation are those that provide greater kinetic energy for this conversion, or where there is a lesser requirement for kinetic energy to overcome precipitation inhibition (Buhmann and Dreybrodt, 1985; Dreybrodt and Buhmann, 1991; Dreybrodt et al., 1997). Such environments highlighted in previous work include those with relatively high turbulence (e.g. Chen et al., 2004; Dreybrodt and Buhmann, 1991; Kano et al., 1999; Liu et al., 1995; Lorah and Herman, 1988; Lu et al., 2000; Zhang et al., 2001) or those where microbial activity occurs (e.g. Pedley et al., 2009).

Hydrochemistry data from all of the study sites indicate that sufficient degassing of CO_2 from springwater for $CaCO_3$ precipitation does not occur until the water reaches a certain point in spring tail. This point is specified by SI_c values of approximately 1 that are indicative of over-saturation for calcite, pH becoming generally greater than

8 and depletion of Ca^{2+}. Where bore data are available, PCO_2 were 50-70% higher than in the emerging springwater samples, suggesting that CO_2 degassing commences once groundwater enters the spring conduit at depth.

The strong degree of disequilibrium between the water and the atmosphere and the turbulent flow conditions within the tail gutters of the mound resulted in a significant drop of PCO_2, but there was no concomitant decrease of Ca^{2+} to indicate that carbonate precipitation was occurring. This is supported by results from microcosm placement experiments conducted between October 2008 and July 2010 (Chapter 3); no precipitation onto marble, glass or copper tablets placed within pool and tail gutter environments was reported. This is in contrast with the findings of Chen et al. (2004), Dreybrodt and Buhmann (1991), Kano et al. (1999), Liu et al. (1995), Lorah and Herman (1988), Lu et al. (2000) and Zhang et al. (2001), who found a close correlation between the location of peak carbonate precipitation and turbulent conditions.

Instead, the data suggest that modern tufa precipitation at the study sites is largely limited to their tail delta environments. This is the area where substrate surface area contact with water becomes larger, which is important for tufa precipitation as substrate provides nucleation sites for carbonate precipitation and anchorage for calci-microbial communities (Pentecost, 2005). Additionally, the larger air-water surface area aids the escape of CO_2 to atmosphere, which offsets the reduced CO_2 degassing due to the progressively decreasing dissolved CO_2 concentrations.

Both during summer and winter, water loss by evaporation was the smaller portion of evapotranspiration and these losses are largely restricted to the lower tail. Water

losses attributable to evapotranspiration are at their greatest in summer months, when ambient temperatures are highest and hydrophyte growth is most vigorous. The dense vegetation cover not only promotes transpiration but also suppresses evaporation via provision of a windbreak and shade. Similar findings were reported by McCarthy et al. (1991) for the Okavango delta in Botswana. Modelling of the carbonate hydrochemistry suggested that the rate of tufa precipitation is largely insensitive to water loss via evapotranspiration over the part of the wetland sampled (Figures 4.9 and 4.10). In the case of Warburton Spring, factoring in the estimated water loss due to evapotranspiration marginally improved the correlation between modelled and measured alkalinity data towards the end of the traverse (Figure 4.9). At Billa Kalina Spring however, estimated water loss was not significant enough to impart any meaningful influence on the modelled outcome (Figure 4.10). These findings are in contrast to the interpretations of Carthew et al. (2003), Carthew et al. (2006), Pedley et al. (1996), Pentecost (2005), Radke (1990) and Wright (2000), who suggested that evaporation is an important factor in tufa deposition in semi-arid and arid terrestrial environments.

Williams and Holmes (1978) used an energy balance method to estimate a summertime evaporation rate at Dalhousie Springs of 6.5 mm/day. However, Holmes et al. (1981) maintained reservations about the accuracy of the Williams and Holmes (1978) model for estimating spring flow as applied to springs in the Lake Eyre South region, approximately 300 km to the south of Dalhousie Springs, because the evaporation rates required to explain the observed wetland sizes were unrealistically high (up to 100 mm/day). This study supports those reservations with respect to evaporation, and it is hypothesised that infiltration is significant in dictating the size

of the wetland. There is ample evidence to suggest that infiltration is occurring. The aeolian and alluvial sediments and gravelly soils surrounding springs are permeable, and water level measurements by Holmes et al. (1981) in temporary shallow piezometers showed the existence of radial subsurface flow beneath the Warburton Spring wetland, which can only be maintained by ongoing infiltration.

The difference between observed Ca^{2+} in water and modelled Ca^{2+} at Warburton Spring is the largest discrepancy within the models. Additionally, the inference concerning the lack of carbonate precipitation from measured Ca^{2+} also stands in contrast to the results from field-based experimental data presented in Chapter 3 in which tufa precipitation rates of up to 1.6 $kg \cdot m^2$/year were directly measured between sample sites 4 and 6. This discrepancy may be the result of a number of factors. The relatively low ratio between surface area exposure and water volume compared to the lower reaches of the tail may be partly responsible for the limited impact observed in corresponding Ca^{2+}. This can be demonstrated by comparing the tail area in which samples sites 4, 5 and 6 are located to that part of the tail occupied by samples sites 7 and 8, which is approximately double. Additionally, field observations such as the presence of an incised tail gutter or "break-out" and experimental data were used in Chapter 3 to argue that calcite dissolution and/or erosion and not precipitation were occurring between the spring vent and the upper tail delta. It is noted that the discrepancy is most reflected in Ca^{2+}, which during carbonate precipitation transfers from solution to the solid phase, as opposed to other constituents such as CO_2, alkalinity and pH, which are affected by gaseous flux to atmosphere. This observation, combined with the location of the discrepancy in samples collected closest to the transition between net carbonate dissolution and net

precipitation, where flow velocity is likely to be greatest and the relatively short distances between samples, it is hypothesised that the Ca^{2+} results obtained may be partly reflective of conditions upstream of where the sample was collected as opposed to constituents where the effects of gaseous flux may provide a more instantaneous change.

Given the composition of the mound structures, hydrochemistry data presented here implies that tufa precipitation has migrated downstream since initial mound formation. A conceptual model describing this migration is presented in Chapter 3, where it was inferred that the CO_2 degassing rate within the pool water will slow concomitant with growth of the mound barrage structure. This slowing is caused by dampening of water turbulence and reduced surface area to volume ratio of the water. Eventually, CO_2 degassing slows sufficiently that $CaCO_3$ under-saturation of pool waters occurs and a breach of the mound (tail gutter or "break-out" development) follows. Carbonate precipitation then migrates to a tail delta environment, or if discharge is sufficiently slow, may also occur on the mound barrage structure but in a lobate form.

The observed slight increase in PCO_2 and corresponding decrease in pH in samples collected from the lower tail environments has been interpreted to be re-invasion of CO_2 from processes responsible for net heterotrophy. The lower tail of spring discharge environments is generally characterised by a shallow, waterlogged marsh and would therefore seem an appropriate environment to assume heterotrophic metabolism to be occurring. The amounts of CO_2 added to the model represent a small fraction of average soil respiration for various vegetation types worldwide (Raich and Schlesinger, 1992) and therefore seem plausible.

Although the data provided adequately dismisses the role of transpiration as a means of promoting CaCO3 precipitation within the portions of wetland examined, the data was insufficient with respect to determining if there was a variance diurnally in accordance with previous authors assessing photosynthesis or other biological processes as a mechanism for CO_2 degassing (e.g. Liu et al., 2006; Liu et al., 2008; Pedley 1994; Pentecost and Coletta, 2007; Spiro and Pentecost, 1991). Additionally, petrological and experimental data presented in Chapter 3 suggests calci-fixating microbes play an important role with respect to the accumulation of $CaCO_3$ as tufa, rather than in some other form of lithofacies. Consequently, the role of biomediation in promoting the precipitation of tufa in mound spring wetland environments, beyond that of providing additional nucleation sites cannot be dismissed.

4.6 Conclusions

This study concludes that there are a number of critical environmental features pertinent to carbonate formation and evolution of mound springs. The first is that most CO_2 degassing from water occurs subsurface within the fracture system that forms the spring conduit, as evidenced by the large decrease in PCO_2 values observed between samples collected at the spring pool to those collected from nearby bores. CO_2 degassing continues after emergence in the upper tail environment where the driving force (i.e., the difference between dissolved and atmospheric PCO_2) and the kinetic energy due to the turbulent flow conditions are highest.

Although water turbulence in other calcareous spring environments commonly coincided with the zone of peak carbonate precipitation (e.g. Liu et al., 1995; Lorah and Herman, 1988; Lu et al., 2000; Zhang et al., 2001), the most turbulent section of water flow within the spring environments studied occurs before the point where tufa

precipitation commences. Instead, tufa precipitation was found to largely occur within the tail delta. This part of the spring wetland is characterised by a large increase in surface area exposure of water to both substrate and the atmosphere. In addition, pH conditions within the tail environment are alkaline, as opposed to the acidic or near neutral conditions found in the vicinity of the spring vent; such conditions are considered by Goulder (1988) and Pedley (1994) to be more conducive to the microbial mediation of $CaCO_3$ precipitation. These conditions are believed to promote tufa precipitation and serve to offset the reduced importance of CO_2 degassing via turbulence as a driving mechanism for $CaCO_3$ precipitation.

Despite the location of the studied wetlands in an arid environment, results demonstrate that evaporation does not play a major role in promoting tufa precipitation in the modern spring environment. Mass balance calculations using Cl^- and stable isotopes indicate that transpiration is more significant than evaporation and that most evapotranspiration occurs within the lower reaches of the wetland, long after $CaCO_3$ precipitation commences.

The water balance model developed for hydrochemical modelling purposes could also be used to suggest the impact of infiltration on the spatial extent of spring supported wetlands and in doing so, lends support to the model developed by Williams and Holmes (1978) for predicting discharge rates via the area of the resultant wetland. The potential role of infiltration in the hydrology of mound springs has not previously been highlighted to this extent.

The negative to near-zero SI_c values found in the spring vent locations and the constancy of Ca^{2+} in the tail gutters, show that carbonate precipitation is not actively

occurring in this zone at present, whereas the occurrence of relict tufa shows that in the past it was. This suggests that during the lifetime of a mound spring, the zone of active carbonate deposition may shift away from near the vent to the tail delta and as such provides supporting hydrochemical evidence for the conceptual model presented in Chapter 3. Conceptual models of spring carbonate formation in other areas should recognise the dynamic character of the depositional environments and should be based on a comprehensive analysis of sediment and water chemistry data. Numerical modelling proved useful in this study to discriminate between the processes that control carbonate precipitation, and provides a generalised framework that can be applied to studies of similar environments elsewhere.